Biochimica et Biophysica Acta 1832 (2013) 2085–2096

Contents lists available at ScienceDirect

Biochimica et Biophysica Acta

journal homepage: www.elsevier.com/locate/bbadis

Negative modulation of mitochondrial oxidative phosphorylation by epigallocatechin-3 gallate leads to growth arrest and apoptosis in human malignant pleural mesothelioma cells

Daniela Valenti [a,*], Lidia de Bari [a], Gabriella Arcangela Manente [b], Leonardo Rossi [c], Luciano Mutti [d], Laura Moro [b], Rosa Anna Vacca [a,*]

[a] Institute of Biomembranes and Bioenergetics, National Council of Research, Bari, Italy
[b] Department of Pharmaceutical Sciences, University of Piemonte Orientale "A. Avogadro", Novara, Italy
[c] Department of Clinical and Experimental Medicine, University of Pisa, Italy
[d] Department of General Medicine, Vercelli-Borgosesia Hospitals, Vercelli, Italy

ARTICLE INFO

Article history:
Received 1 April 2013
Received in revised form 11 July 2013
Accepted 23 July 2013
Available online 2 August 2013

Keywords:
EGCG
Malignant mesothelioma
Mitochondria
OXPHOS inhibition
STAT3

ABSTRACT

Increasing evidence reveals a large dependency of epithelial cancer cells on oxidative phosphorylation (OXPHOS) for energy production. In this study we tested the potential of epigallocatechin-3-gallate (EGCG), a natural polyphenol known to target mitochondria, in inducing OXPHOS impairment and cell energy deficit in human epithelioid (REN cells) and biphasic (MSTO-211H cells) malignant pleural mesothelioma (MMe), a rare but highly aggressive tumor with high unmet need for treatment. Due to EGCG instability that causes H_2O_2 formation in culture medium, the drug was added to MMe cells in the presence of exogenous superoxide dismutase and catalase, already proved to stabilize the EGCG molecule and prevent EGCG-dependent reactive oxygen species formation. We show that under these experimental conditions, EGCG causes the selective arrest of MMe cell growth with respect to normal mesothelial cells and the induction of mitochondria-mediated apoptosis, as revealed by early mitochondrial ultrastructure modification, swelling and cytochrome *c* release. We disclose a novel mechanism by which EGCG induces apoptosis through the impairment of mitochondrial respiratory chain complexes, particularly of complex I, II and ATP synthase. This induces a strong reduction in ATP production by OXPHOS, that is not adequately counterbalanced by glycolytic shift, resulting in cell energy deficit, cell cycle arrest and apoptosis. The EGCG-dependent negative modulation of mitochondrial energy metabolism, selective for cancer cells, gives an important input for the development of novel pharmacological strategies for MMe.

1. Introduction

Mitochondrial bioenergetics and dynamics and their proper regulation are crucial for tumor cell growth. Under normal conditions, cells rely on mitochondrial oxidative phosphorylation (OXPHOS) to provide energy for cellular activities. Cancer cells are generally characterized by a strong enhancement of aerobic glycolysis, the so-called Warburg effect, often associated to the decrease in mitochondrial respiration and OXPHOS [1]. However, it is becoming increasingly evident that enhanced OXPHOS occurs in a variety of tumors and consequently mitochondria could be a promising target for the development of efficient anticancer therapies [2–4].

Consistently, it has been recently reported that mitochondria-targeted molecules, able to disrupt mitochondrial architecture and induce swelling, are effective to reduce the growth of epithelial tumor cells, such as human breast cancers [5] and malignant mesothelioma (MMe) [6]. MMe is a rare, but with an increasing incidence, insidious and highly aggressive cancer with poor prognosis [7]; due to its high drug resistance, despite the reported improvements in the clinical management, the unmet need for malignant mesothelioma treatment is high. Thus, in the light of current failures in MMe therapies, attempts to induce cell energy deficit can be an attractive strategy to reduce MMe tumor growth.

In this study we aimed at determining whether epigallocatechin-3-gallate (EGCG), known to be a mitochondrial-targeted drug [8,9], is able to induce mitochondrial energy deficit and a selective growth arrest of MMe cells. EGCG, a natural polyphenol component of green tea, has been extensively studied for its anticarcinogenic effect in a wide variety of cancer cells (for Refs. see [10]) and it has been shown

Abbreviations: CAT, catalase; cyt *c*, cytochrome *c*; DCF, dichlorofluorescein; DCFH-DA, 2′,7′-dichlorofluorescein diacetate; EGCG, epigallocatechin-3-gallate; GLU, glutamate; MAL, malate; MMe, malignant mesothelioma; MRC, mitochondrial respiratory chain; OXPHOS, oxidative phosphorylation; ROS, reactive oxygen species; SOD, superoxide dismutase; STAT3, phospho-signal transducer and activator of transcription 3; SUCC, succinate; XTT, 3-(4,5-dimethylthiazol-2-yl)-2,5-diphenyltetrazolium bromide.

* Corresponding authors. Tel.: +39 80 5443380.
E-mail addresses: d.valenti@ibbe.cnr.it (D. Valenti), r.vacca@ibbe.cnr.it (R.A. Vacca).

0925-4439/$ – see front matter © 2013 Elsevier B.V. All rights reserved.
http://dx.doi.org/10.1016/j.bbadis.2013.07.014

to interact with a large set of protein targets [11] modulating a variety of cell signaling pathways (for Refs. see [12]). Although EGCG targets mitochondria in tumor cells [9], little is known about the effect of EGCG on mitochondrial function in cancer [13,14].

Another open question is the proper use of EGCG for *in vitro* studies necessary to characterize its mechanism of action. It has been shown that EGCG induces apoptosis in a variety of cultured cancer cell types, including MMe cells, through its pro-oxidant activity [15–18]. However, there is evidence that some of the cytotoxic effects of this compound may be related to its instability under culture conditions, since, as a result of its auto-oxidation, oxidative products and reactive oxygen species (ROS) are formed in the extracellular phase. The addition of superoxide dismutase (SOD) and catalase (CAT) to the culture medium has been shown to stabilize EGCG and to increase its half-life to more than 24 h [19–21].

In this study, we emphasize the need to stabilize EGCG in order to obtain a selective inhibitory action on human MMe-derived REN cells. Our results disclose for the first time a novel mechanism by which EGCG, through the early impairment of mitochondrial respiratory chain (MRC) complexes and ATP synthase, induces a strong cell energy deficit followed by cell cycle arrest in G2/M phase and mitochondria-mediated apoptosis in MMe cells.

2. Materials and methods

2.1. Cell cultures and materials

The epithelioid MMe derived REN cell line, used as the principal experimental model in this investigation, is a tumourigenic, p53-mutant, epithelial subtype [22]. It was characterized and kindly provided by Dr. Albelda S.M. (University of Pennsylvania, Philadelphia; PA) and characterized [23]. MSTO-211H, derived from biphasic mesothelioma, and mesothelial MET5A cell lines were obtained from Istituto Scientifico Tumori (IST) Cell-bank, Genoa, Italy. Cells were cultured at 37 °C in humidified 5% CO_2/95% air in RPMI 1640 medium (GIBCO/BRL) supplemented with 10% heat-inactivated fetal bovine serum (GIBCO/BRL), 2 mM L-glutamine, penicillin (100 units/ml) and streptomycin (100 μg/ml) (GIBCO/BRL). Cells were subjected to a 1:3 split every 3 days.

All reagents used were from Sigma-Aldrich unless otherwise specified.

2.2. EGCG treatment

EGCG – extracted from green tea leaves with a purity >95% (Sigma-Aldrich) – was freshly prepared for each experiment at 20 mM concentration in PBS. Cells were seeded into 10-cm Petri dishes, 6-well or 96-well plates, according to the experiment, and cultured until they have reached 60–70% confluence (about 24 h). For dose-dependent experiments, cells were treated with EGCG (from 20 to 200 μM) added to the fresh culture medium for 24 h in the absence or presence of SOD (5 units/ml) and CAT (30 units/ml) [20]. For time-dependent experiments, the medium containing 100 μM EGCG plus SOD and CAT was replaced after 24 h of incubation.

2.3. Proliferation assays

Cell proliferation assay was performed by using 3-(4,5-dimethylthiazol-2-yl)-2,5-diphenyltetrazolium bromide reagent (XTT, Cell Proliferation Kit II, Roche). 6000 cells per well were seeded into a 96-well plate and incubated over-night at 37 °C in a CO_2 incubator to allow adherence. To assay cell proliferation, 50 μl of XTT labeling mixture were added to each well and the plate incubated at 37 °C for 2–4 h following the manufacturer's instructions. Formazan dye accumulation produced by metabolically active cells was monitored by reading absorbance at 490 nm, with a reference wavelength at 655 nm, by using the microplate reader mod. 680 (Bio-Rad).

For cell count experiments, cells were seeded at a density of 1×10^6 cells in 10 cm culture plates and incubated over-night at 37 °C. Cells were then trypsinized, stained with Trypan blue and counted in a Bürker haemocytometer within 5 min after staining.

2.4. ROS detection

The pro-oxidant dose-dependent response of EGCG was checked by measuring H_2O_2 concentration in the culture medium after 1 h of incubation with different EGCG concentrations either in the absence or presence of SOD (5 units/ml) plus CAT (30 units/ml), by using Amplex® Red Hydrogen Peroxide/Peroxidase Assay Kit (Molecular Probes).

Quantitative analysis of intracellular ROS was performed by means of an LS50 Perkin Elmer spectrofluorimeter, using 2′,7′-dichlorofluorescein diacetate (DCFH-DA), a non-fluorescent dye which is hydrolyzed inside the cells and reacts with multiple types of ROS, mainly H_2O_2, to give the fluorescent product, dichlorofluorescein (DCF) [24]. Cultured cells were incubated with 5 μM DCFH-DA for 30 min under growth conditions, washed and suspended in PBS. Fluorescence emission was recorded at the excitation–emission wavelengths of 488 and 520 nm, respectively and normalized to the protein content to determine the relative ROS production. Protein concentration was quantified by using a modified Bradford assay (Bio-Rad protein assay) according to the manufacturer's instructions.

ROS were visualized in live REN cells by using laser scanning confocal microscopy imaging. Cells were cultured at low density on fibronectin-coated 35-mm glass-bottom dishes and treated with 100 μM EGCG in the presence or absence of SOD and CAT. After 24 h, cells were incubated for 20 min at 37 °C with both 3 μM DCFH-DA and 3 μM MitoSOX™ (Molecular Probes), a selective mitochondria-targeted probe, specific for superoxide anion [25]. After washing with PBS, stained cells were examined under a Leica TCS SP5 II microscope (images collected using a 60× objective). The green fluorescence of oxidized DCF was analyzed by exciting the sample with a Diode 405 laser (λex 488 nm); the red fluorescence of MitoSOX was analyzed by exciting the sample with a HeNe laser 543 (λex 543 nm).

2.5. Cell cycle analysis

Cell cycle analysis was carried out by seeding 5×10^5 cells per well in 96-well cell culture plates in the presence or in the absence of 100 μM EGCG plus SOD (5 U/ml) and CAT (30 U/ml) for 1, 3, 6, 18 and 24 h at 37 °C in a 5% CO_2 atmosphere.

After incubation, adherent cells were detached with trypsin (0.5% trypsin/0.1% EDTA in PBS), harvested in complete RPMI and centrifuged at 500 ×*g* for 10 min. Pellets were washed with PBS and fixed with ice-cold 75% ethanol overnight at 4 °C, treated with 100 μg/ml RNase A, and subsequently stained with 25 μg/ml propidium iodide. Samples were analyzed by using a flow cytometer FACS (Becton Dickinson) and ModFit software (Verity Software House).

2.6. Apoptosis assessment

Cells were plated in 96-well culture plates at 6000 cells per well and incubated over-night at 37 °C in a CO_2 incubator to allow adherence. After 24 h, cells were exposed to EGCG in a culture medium containing SOD and CAT for an additional 48 h. Apoptosis was measured with the Cell Death Detection ELISA (Roche), which was performed according to the manufacturer's protocol. The amount of histone-associated-DNA-fragments (mono- and oligonucleosomes) was assayed in the cytoplasmic cell fraction by measuring absorbance at 405 nm, with a reference wavelength at 655 nm, using the microplate reader mod. 680 (Bio-Rad).

2.7. Immunoblot analysis

Cells were lysed with 0.1% Triton X-100 in PBS in the presence of a protease inhibitor cocktail (Sigma-Aldrich). Cell lysates (0.05 mg protein) were resolved by a 10%–12% SDS-polyacrylamide gel (depending on the molecular weight) and transferred to a polyvinylidene difluoride membrane (Millipore). Membranes were blocked with TBS-T (50 mM Tris, 150 mM NaCl, 0.02% Tween 20, pH 7.5) containing 5% non-fat milk and probed with primary antibodies overnight at 4 °C. Immunoblot analysis was performed, essentially as described in [26], using horseradish peroxidase-conjugated anti-mouse or anti-rabbit antibodies and enhanced chemiluminescence Western blotting reagents (Amersham, Pharmacia Biotech). Membranes were also probed with anti-β-actin antibody as internal loading control and densitometry values of immunoreactive bands for each sample were normalized versus the corresponding densitometry value of β-actin.

2.8. Preparation of mitochondrial and cytoplasmic protein fractions

Cells were trypsinized, washed with ice-cold PBS and centrifuged at 800 ×*g* for 5 min. Cell pellets were lysed in Buffer A consisting of 20 mM HEPES-Tris (pH 7.6), 10 mM KCl, 1.5 mM $MgCl_2$, 0.1 mM EGTA, 0.1 mM EDTA, 1 mM dithiothreitol, 250 mM sucrose, 10 μg/ml aprotinin, 10 μg/ml leupeptin, 10 mM benzamidine, 1 mM phenylmethylsulfonyl fluoride (PMSF), and 0.2 mM sodium orthovanadate. Samples were then homogenized with a Dounce homogenizer (20 strokes for 30 min on ice) and centrifuged twice at 2000 ×*g* for 5 min to remove nuclei and unlysed cells. The final supernatant was centrifuged at 13,000 ×*g* for 15 min to obtain the mitochondrial fraction (pellet) and the cytosolic fraction (supernatant).

Supernatants were then centrifuged at 10,000 ×*g* for 90 min, to obtain a clean cytosolic fraction, while the mitochondrial fraction was solubilised in Buffer B (1% Triton X-100, 10 mM Tris-HCl (pH 7.4), 150 mM NaCl, 5 mM EDTA, 10 μg/ml of aprotinin, 10 μg/ml of leupeptin, 10 mM benzamidine, 1 mM PMSF and 0.2 mM sodium orthovanadate) for 30 min on ice.

Mitochondrial and cytosolic fractions were centrifuged at 13,000 ×*g* for 10 min and the supernatants were collected and assayed for protein concentration with the Bio-Rad protein assay method (Bio-Rad). Both fractions were separated by SDS-PAGE under reducing conditions and immunoblot analysis was performed as described above.

2.9. Transmission electron microscopy

REN cells were incubated with 100 μM EGCG plus SOD and CAT for 1, 3, 6, 18, 24 or 48 h and then trypsinized and collected by centrifugation. The cellular pellets were washed in PBS and fixed as previously described [27]. Ultrathin sections were placed on Formvar carbon-coated copper grids, stained with uranyl acetate and lead citrate and observed under a JEOL 100 SX transmission electron microscope (JEOL, Ltd, Japan).

2.10. Measurement of MRC complex activities

Measurements of MRC complex activities were carried out in mitochondrial membrane-enriched fractions from cultured cells. Aliquots of trypsinized cells were washed with ice-cold PBS, frozen in liquid nitrogen and kept at −80 °C until use. Isolation of mitochondrial membrane-enriched fractions was carried out as described in [28] and measurement of MRC complex activities performed essentially as in [29], by three assays which rely on the sequential addition of reagents to measure the activities of: i) NADH:ubiquinone oxidoreductase (complex I) followed by ATP synthase (complex V), ii) succinate:ubiquinone oxidoreductase (complex II) and iii) cytochrome *c* oxidase (complex IV) followed by cytochrome *c* oxidoreductase (complex III).

2.11. Measurement of mitochondrial ATP production

Cells were detached from a 10-cm plate by trypsin treatment, washed with PBS and suspended in ice-cold sucrose medium (0.25 M sucrose, 10 mM Tris-HCl pH 7.2, 1 mM EGTA). To measure the mitochondrial ATP production, cells (1 mg of protein) were incubated at 37 °C in 2 ml of the respiration medium (210 mM mannitol, 70 mM sucrose, 20 mM Tris-HCl, 5 mM KH_2PO_4/K_2HPO_4 pH 7.4, 3 mM $MgCl_2$ and 5 mg/ml BSA) and permeabilized with digitonin (0.01% w/v for 5 min). Then the ATP detecting system (2.5 mM glucose, 2 U hexokinase, 1 U glucose 6-phosphate dehydrogenase, 0.25 mM $NADP^+$) was added in the presence of 10 μM diadenosine pentaphosphate (Ap5A), used to inhibit adenylate kinase; the measurement was made in the presence of either glutamate plus malate (GLU/MAL, 5 mM each) or succinate (SUCC, 5 mM) plus rotenone (3 μM), used as respiratory energy sources. Then ADP (0.5 mM) was added and the reduction of $NADP^+$, which reveals ATP formation, was monitored as an increase in absorbance at 340 nm. Care was taken to use enough hexokinase/glucose 6-phosphate dehydrogenase coupled enzymes to ensure a not-limiting ADP-regenerating system for the measurement of ATP production.

2.12. Measurement of cellular ATP content

Cells were detached from a 10-cm plate by trypsin treatment, washed with PBS and cellular ATP content was assayed in cell extracts obtained by the boiling water procedure as described in [30] by enzymatic procedure as described in [31].

2.13. Measurement of extracellular L-lactate levels

REN cells were plated in 5-cm dishes, grown until they reached subconfluence and incubated with 100 μM EGCG plus SOD and CAT for 1, 3, 6, and 24 h. The extracellular L-lactate levels were measured in the culture medium by using the L-lactate dehydrogenase method, which gives a reliable estimate of L-lactate production inside the cells [32].

2.14. Statistical analysis

Statistical evaluation was performed by one way ANOVA and Student's t-test. The threshold for statistical significance was set to $P < 0.05$.

3. Results

3.1. EGCG, stabilized by SOD and CAT, selectively inhibits MMe REN cell growth and impairs mitochondrial bioenergetics in a dose-dependent manner

In order to ascertain the capability of EGCG to selectively inhibit MMe cell growth, we first examined the dose-response effect of EGCG treatment on MMe REN cell proliferation in comparison to that produced on normal mesothelial MET5A cell proliferation, both in the absence or presence of SOD and CAT used to prevent EGCG auto-oxidation [18–21].

As shown in Fig. 1A, 24 h-treatment with EGCG selectively inhibited the growth of the MMe REN cells in a dose-dependent manner when incubated in the presence of SOD/CAT, with an estimated IC_{50} of 100 μM, as measured by XTT assay; conversely, the viability of the normal mesothelial MET5A cells was not affected by EGCG in the presence of SOD/CAT. On the contrary, EGCG proved to inhibit cell growth of both REN and MET5A cells when added in the absence of SOD/CAT (Fig. 1A).

Importantly, in the absence of SOD/CAT, EGCG induced a dose-dependent cell death in both REN and MET5A cells (Fig. 1B). On the contrary in the presence of SOD/CAT, stabilized EGCG was still able to induce cell apoptosis in MMe REN cells at 100 μM and 200 μM, although to a less extent than in the absence of SOD/CAT, but completely loss its pro-apoptotic activity in normal MET5A cells (Fig. 1B).

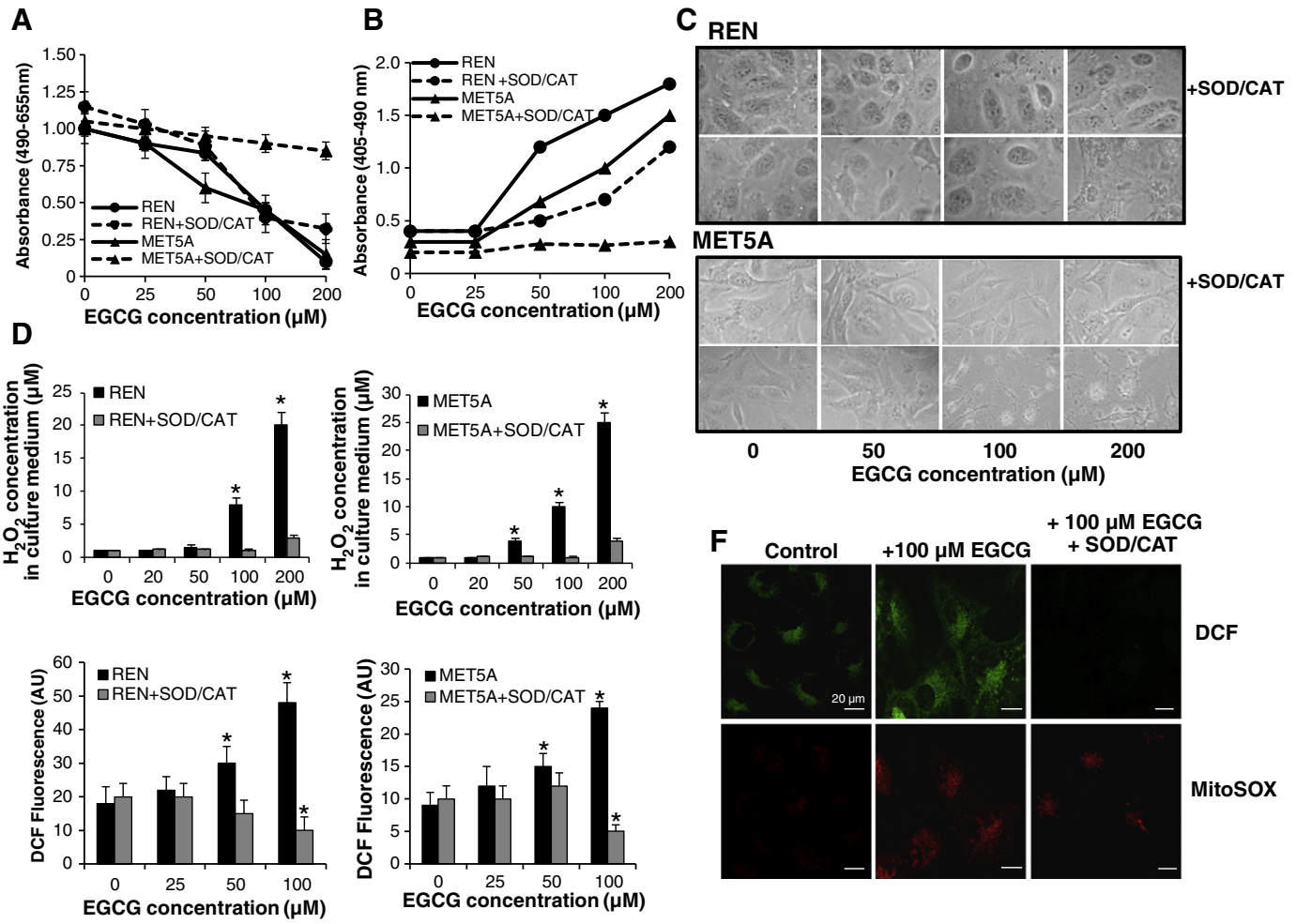

Fig. 1. Dose-response effect of EGCG on REN and MET5A cell proliferation and ROS production in the presence or absence of SOD and CAT. MMe REN and MET5A cells were treated with EGCG at the indicated concentrations either in the absence or presence of SOD (5 U/ml) and CAT (30 U/ml). MMe REN and normal MET5A cells were seeded into 96-well plate and treated for 24 h with EGCG at the indicated concentrations, either in the absence or in the presence (dotted line) of SOD and CAT. Fresh medium was then used to replace the EGCG-containing medium and (A) cell proliferation was analyzed by XTT assay and (B) apoptosis was measured by the Cell Death Detection ELISA assay (Roche). (C) Analysis of cell morphology. Cells were examined and photographed under phase-contrast microscopy (×400). (D) Production of H_2O_2 in both REN and MET5A culture medium after 1 h incubation as a function of EGCG concentration. Each bar represents mean ± SD ($n = 4$) for different H_2O_2 concentrations. (E) Intracellular ROS production in 24 h-treated REN and MET5A cells as a function of EGCG concentration. Cells were stained with 5 μM DCF-DA and quantification of intracellular ROS was reported as the means (±SD) of DCF fluorescence arbitrary units (A.U.) measured by fluorimetric analysis. (F) Confocal microscopy imaging of ROS generation and sub-cellular localization in REN cells treated for 24 h with 100 μM EGCG. Images are superimpositions of 10 confocal z-planes and are representative of typical experiment. Each graph is representative of six independent experiments. Significant differences between untreated and treated cells are indicated with asterisks (* = $P < 0.05$).

Consistently, the phase-contrast microscopy analysis of REN cells treated with 100 or 200 μM EGCG in the absence or presence of SOD/CAT showed a reduction in cell density, several cellular debris and signs of cellular sufferance and in addition, EGCG-treated REN in the absence of SOD/CAT showed several cytoplasmic vacuoles (Fig. 1C). Similar changes occurred in normal MET5A cells treated with EGCG alone, whereas in the presence of SOD/CAT, even up to 200 μM EGCG, cells were well spread and with a flattened morphology, as in non-treated controls.

Since the observed cytotoxic effect of EGCG in the absence of SOD/CAT could depend on ROS production due to its auto-oxidation [17–21], H_2O_2 concentration was measured in the culture medium of both EGCG-treated REN and MET5A cells as a function of EGCG concentration (Fig. 1D). An increase in extracellular H_2O_2 concentration was observed in medium collected from both cell lines starting from 50 to 100 μM EGCG, almost completely prevented by SOD/CAT addition in both cases. Thus, ROS scavenging and the consequent stabilization of EGCG by SOD/CAT in the culture medium, completely prevented EGCG cytotoxicity in normal MET5A cells, but did not reduce the inhibition of MMe REN cell growth (see Fig. 1A).

An increase in intracellular levels of ROS was found in 24 h-treated REN and MET5A cells starting from 50 μM EGCG, as shown by DCF fluorescence measurements; this ROS overproduction was prevented by the addition of exogenous SOD and CAT in both cases (Fig. 1E). The intracellular ROS production was also investigated by confocal microscopy analysis, by incubating REN cells with 100 μM EGCG for 24 h in the absence or presence of SOD/CAT. Both DCF green fluorescence – revealing mainly H_2O_2 production [24] – and MitoSOX red fluorescence – revealing production of superoxide from mitochondria [25] – were already detectable in control cells, and dramatically increased in EGCG-treated REN cells (Fig. 1F). The presence of SOD/CAT completely prevented the cytoplasmic ROS accumulation, while the EGCG-triggered overproduction of superoxide anion by mitochondria remained still substantial.

Since it is well established that the impairment of the mitochondrial respiratory chain complexes, in particular complexes I and III, induces superoxide anion formation [33], we hypothesized that the overproduction of mitochondrial ROS in REN cells treated with EGCG stabilized by SOD/CAT (see Fig. 1E) was a consequence of an EGCG-mediated mitochondrial dysfunction. The functional analysis of the mitochondrial respiratory

chain (MRC) complexes revealed a generalized dose-dependent decline in complex activities 24 h after the treatment of REN cells with EGCG stabilized by SOD/CAT (Fig. 2A). Moreover, a remarkable decline in ATP production via mitochondrial OXPHOS was observed upon the addition of the respiratory substrates GLU/MAL or SUCC (Fig. 2B). In addition, the cellular ATP level was decreased in a dose-dependent manner by the stabilized EGCG, becoming 50% lower than that of the untreated cells, with 100 μM EGCG (Fig. 2C). It is interesting to note that no change in both MRC complex activities and ATP cellular level was observed in normal MET5A cells incubated with 100 μM EGCG stabilized with SOD/CAT (not shown).

Altogether these data demonstrate that a 24 h-treatment of REN cells with stabilized 100 μM EGCG, induces a significant impairment of the MRC function and a decline in the ATP production, selectively in MMe REN cells.

All the further analysis of EGCG-dependent effects on MMe cells were carried out incubating REN cell with 100 μM EGCG in the presence of SOD and CAT.

3.2. EGCG induces cell cycle arrest in G2/M phase and mitochondria-mediated apoptosis in MMe REN cells

To further investigate EGCG-dependent growth inhibition in MMe REN cells, cell cycle distribution analysis was performed during the 24-hour period of EGCG treatment (Fig. 3A). In an early phase (1–6 h) of the treatment no significant changes were observed in cell cycle distribution with respect to untreated control cells, after 18/24 h, instead, the REN surviving population in G2/M phase increased about 3-fold as compared to untreated cells whose G2/M phase population remained unchanged during all the time period investigated (not shown). The arrest in G2/M was associated with a concomitant decrease in the percentage of cells in G0/G1 phase (Fig. 3A).

In parallel, we also evaluated the cell number and apoptosis in EGCG treated REN cells. After prolonged exposure to EGCG (48 h), a 2-fold decrease in cell number (Fig. 3B) and an increase in cell apoptosis (Fig. 3C) occurred with respect to untreated cells.

Since mitochondria are known to play a central role in eliciting apoptosis in response to many triggers, including EGCG [13,34,35] and being the mitochondrial release of cytochrome *c* (cyt *c*) an early step in the time course of the events leading to mitochondria-mediated apoptosis [36], we analyzed the distribution of cyt *c* between mitochondrial and cytosolic fractions during the 24 hour period of EGCG-treatment in REN cells. The release of cyt *c* from mitochondria to the cytosol started 6 h after EGCG addition. Cytosolic cyt *c* level reached about 3-fold with respect to controls 24 h after the treatment, as shown by immunoblotting analysis (Fig. 3D and E).

Ultrastructural observations under transmission electron microscope have been performed to analyze the early and late effects of EGCG treatment on subcellular cytoarchitecture and mitochondria. Control REN cells (treated with SOD/CAT from 1 to 48 h) showed an electron dense cytoplasm rich in ribosomes with several mitochondria, one or two Golgi apparatus and rare endoplasmic reticulum cisternae (Fig. 4 A, B). Most of mitochondria showed a dense expanded matrix and medium/small intracristae compartments, which extend parallel to the organelle main axis (Fig. 4 A, B). No ultrastructural differences with respect to controls were observed in REN cells treated with the stabilized EGCG for 1 h (data not shown). Differently, 6 h after treatment, an accurate analysis of mitochondrial morphology revealed an initial

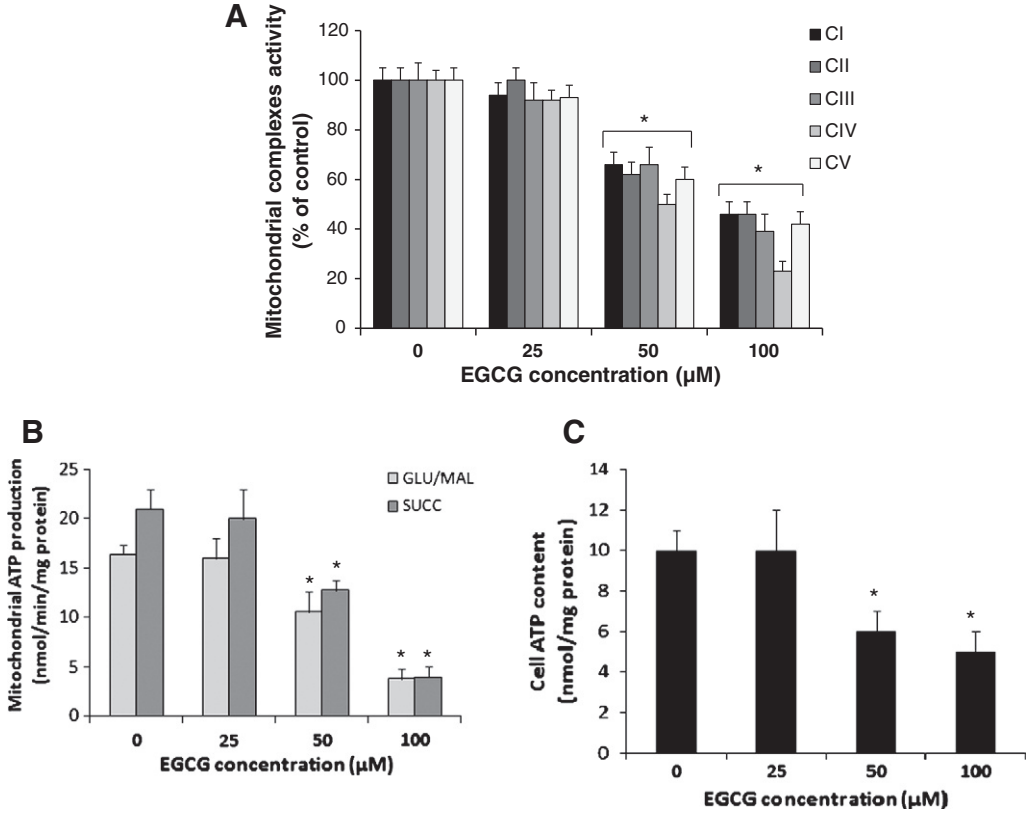

Fig. 2. Dose-dependent effect of stabilized EGCG on MRC complex activities, mitochondrial ATP synthesis and cellular ATP content in MMe REN cells. MMe REN cells were treated for 24 h with EGCG at the indicated concentrations in presence of SOD and CAT. (A) The activities of CI (complex I, NADH:ubiquinone oxidoreductase), CII (complex II, succinate:ubiquinone oxidoreductase), CIII (complex III, cytochrome *c* reductase), CIV (complex IV, cytochrome *c* oxidase) and CV (complex V, ATP synthase) were measured spectrophotometrically and are expressed as a percentage with respect to untreated control REN cells. (B) The rate of mitochondrial ATP synthesis was measured spectrophotometrically and expressed as nmol/min/mg protein. (C) The levels of cellular ATP are expressed as nmol/mg cell protein. Each graph is representative of six independent experiments. Each bar represents mean ± SD. Significant differences between untreated and treated cells are indicated with asterisks (* = $P < 0.05$).

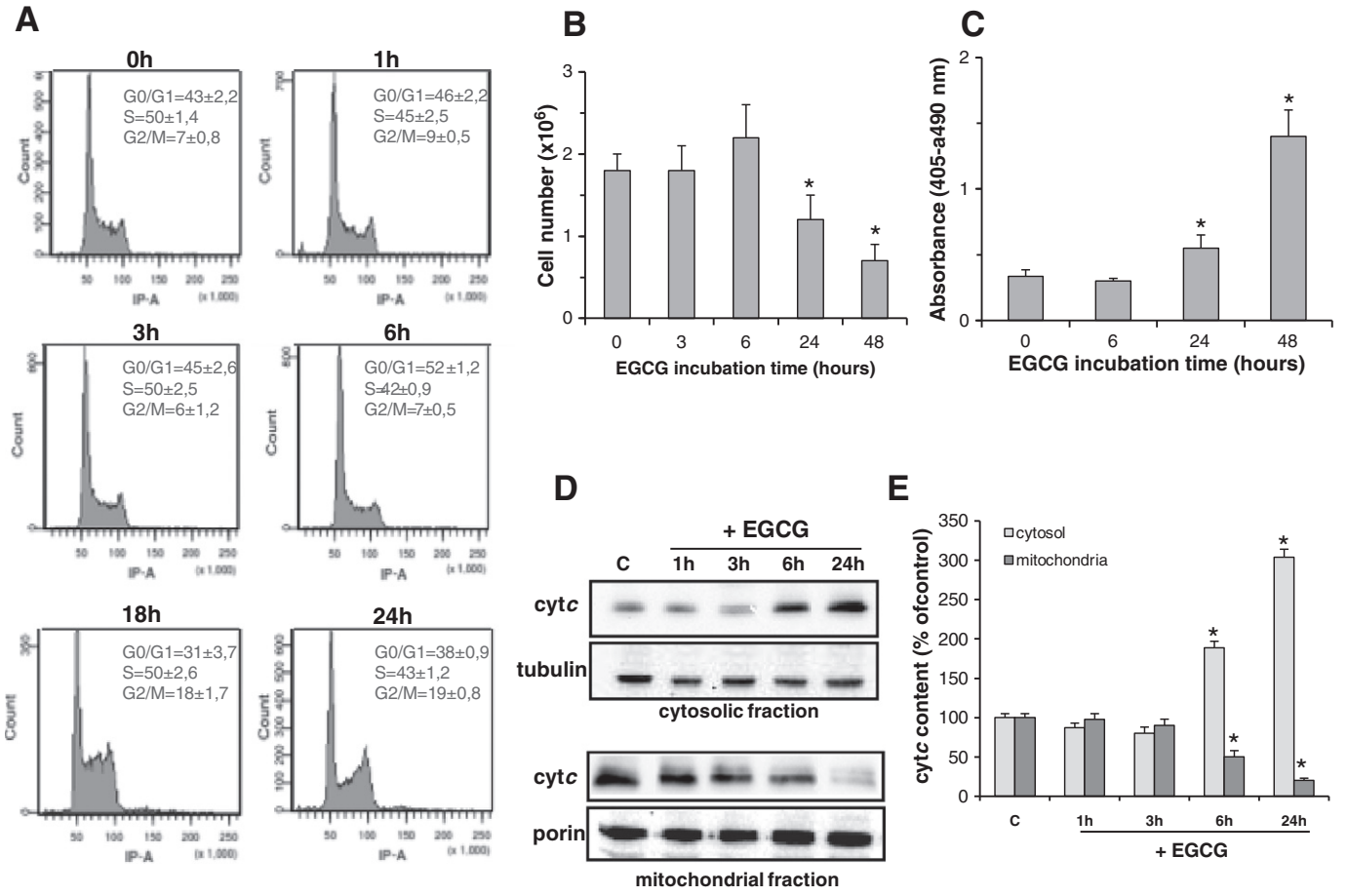

Fig. 3. Stabilized EGCG induces cell cycle arrest and apoptosis in MMe REN cells. MMe REN cells were treated with 100 μM EGCG in presence of SOD and CAT and collected at the indicated time periods. (A) DNA histograms indicate cell cycle kinetics. The percentage of cells in G1/G0, S and G2/M phases is indicated. Data shown are representative of three independent experiments. (B) Cell survival at different times. Graph is representative of six independent experiments. (C) Cell apoptosis measured with the Cell Death Detection ELISA (Roche), which detects DNA fragments within immunocaptured nucleosomes. Graph is representative of three independent experiments. (D) Representative immunoblotting and (E) densitomentric analysis of cyt *c* measured in the cytosolic (0.05 mg protein) and mitochondrial (0.02 mg protein) fractions prepared from REN cells; protein levels of tubulin and porin as cytosolic and mitochondrial protein markers, respectively, were also analyzed. The levels of cyt *c* in mitochondrial ad cytosolic fractions, normalized *vs* the respective loading control proteins, are expressed as the percentage versus untreated control cells which remained constant during the incubation time. Graph is representative of six independent experiments. Each bar represents mean ± SD. Significant differences between untreated and treated cells are indicated with asterisks (* = $P < 0.05$).

cristae remodeling prevalently consisting in cristae opening and in the formation of larger intracristae spaces (Fig. 4C). No additional subcellular alterations were observable in these samples. Interestingly, 18 h after the treatment mitochondria ultrastructure resulted highly altered with almost all mitochondria larger in size with highly enlarged intracristae compartment (Fig. 4D). 24 h after the treatment some of the enlarged mitochondria showed pale matrix and in some cases totally disrupted or profoundly disorganized cristae (Fig. 4E, arrows). These morphological alterations are ascribable to swollen mitochondria that have lost membrane integrity. Other mitochondria, although provided with an electrondense matrix, showed marked cristae reorganization, in particular vesicular cristae that do not attach to the peripheral inner membrane were observable (Fig. 4E, arrowheads). Finally, 48 h after the treatment the majority of cells showed clear sign of chromatin margination a typical feature of apoptotic cell death (Fig. 4F), to confirm the data shown in Fig. 3C.

3.3. EGCG early affects activity and protein levels of MRC complexes inducing MMe REN cell energy deficit

The early ultrastructural modification of mitochondria occurring at 6 h after EGCG treatment (see Fig. 4), when neither changes in REN cell growth nor cell apoptosis were observed (see Fig. 3 A–C), prompted us to investigate whether EGCG caused early specific alterations in the mitochondrial functions. The measurement of MRC complex activities in mitochondrial membrane-enriched fractions from EGCG-treated REN cells during the 24 hour period of treatment showed that a significant reduction in MCR activity already occurred 3 h after the treatment for complex I, II, IV and ATP synthase (complex V). The activity of all complexes was reduced of about 50% 18–24 h after the treatment (Fig. 5A).

To verify whether the EGCG inhibitory effect on the activity of MRC complexes was associated with changes in their content, the levels of some OXPHOS complex subunits were analyzed (Fig. 5B). In line with the functional data, a shared pattern of decrease in the levels of subunits of all OXPHOS complexes was observed in EGCG-treated REN cells starting from 3 h after EGCG incubation and involving particularly the subunits of complexes I, II and V (Fig. 5C), as well as complex IV, as shown in a representative immunoblot (Fig. 5B), and in the statistical analysis of densitometry values (Fig. 5C).

To give some insight into the molecular basis of this early MRC complexes deficit in EGCG-treated REN cells, we investigated the protein levels of the phospho-signal transducer and activator of transcription 3 (STAT3) that is known to regulate MRC complex expression and activity [37] and has been recently reported to be down-regulated by EGCG in human pancreatic cancer cells [38]. Interestingly, as shown by the

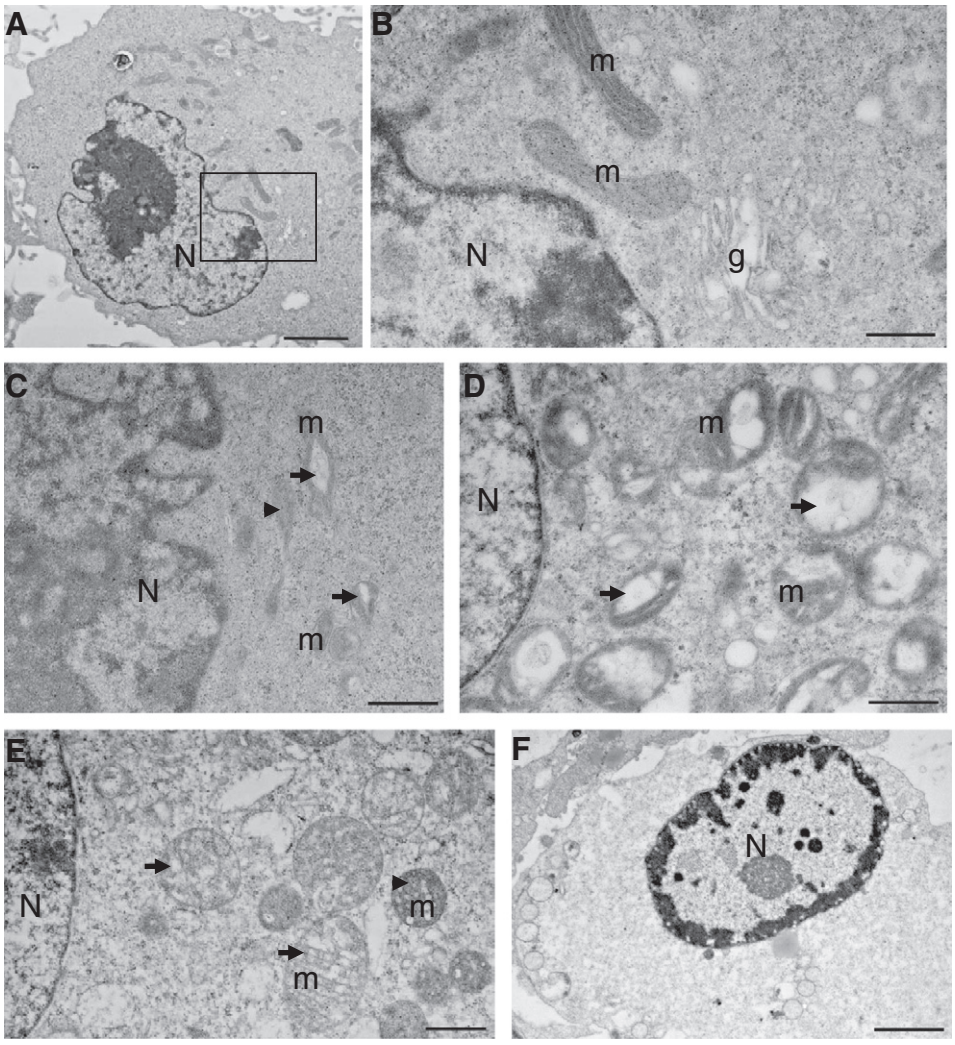

Fig. 4. Ultrastructural analysis of REN cells treated with stabilized EGCG. (A) A control cell treated with SOD/CAT for 24 h. N: nucleus, scale bar: 2 μM. (B) Magnification of the region boxed in fig. A showing two mitochondria (m), a Golgi apparatus (g) and a portion of the nucleus (N). Scale bar: 0.5 μM. (C) Detail of a cell treated with SOD/CAT and 100 μM EGCG for 3 h. Both normally shaped mitochondria (arrowheads) and mitochondria showing signs of cristae opening (arrows) are visible. m: mitochondria, N: nucleus, scale bar: 0.66 μM. (D) Detail of a cell treated with SOD/CAT and 100 μM EGCG for 18 h. Large mitochondria with clear signs of cristae disorganization (arrows) are visible. m: mitochondria, N: nucleus, scale bar: 0.66 μM. (E) Detail of a cell treated with SOD/CAT and 100 μM EGCG for 24 h. Both swollen mitochondria (arrows) and mitochondria showing cristae reorganization (arrowheads) are visible. m: mitochondria, N: nucleus, scale bar: 0.66 μM. (F) A cell showing condensation and margination of nuclear chromatin 48 h after the treatment with stabilized EGCG. N: nucleus, scale bar 2.5 μM.

immunoblot analysis (Fig. 5D and E), a 50% decrease in STAT3 protein level was found starting from 3 h after treatment with EGCG with respect to untreated REN cells.

To assess whether the alterations in MRC complex activities and protein level have consequences on energy status, the cellular ATP level was measured in EGCG-treated REN cells. Interestingly, a marked elevation of cellular ATP amount was found 1 h after EGCG treatment and was maintained up to 3 h. The ATP amount then gradually declined, dropping under the level of controls at 24 h (Fig. 6A). This drug-induced ATP surge is not unusual in cells *en route* to apoptosis and could derive from both OXPHOS and anaerobic glycolysis [39,40]. To check this, we measured both the mitochondrial ATP production and the extracellular release of L-lactate, the end-product of glycolysis, as a function of EGCG incubation time. We found that the rate of mitochondrial ATP production induced by complexes I and II substrates (MAL/GLU and SUCC, respectively) increased after 1 h of EGCG incubation and progressively decreased thereafter, declining under control values at 3 h of incubation (Fig. 6B). In parallel, we found that levels of L-lactate strongly increased after 3 h of EGCG treatment (insert of Fig. 6C) remaining slightly higher with respect to untreated cells at all the following incubation times (Fig. 6C).

3.4. EGCG inhibits mitochondrial metabolism inducing cell energy deficit and apoptosis in biphasic MMe MSTO-211H cells

In order to confirm the efficacy of EGCG on MMe cell proliferation and the molecular mechanism by which it acts in these cells, we checked whether and how 100 μM EGCG stabilized with SOD/CAT induces cell death in MSTO-211H, a biphasic malignant cell line more aggressive than the other MMe cells [41].

Similarly to REN cells, the exposure of MSTO-211H to EGCG up to 48 h inhibited cell growth (Fig. 7A) and determined an increase in cell apoptosis as compared to untreated cells of 1.6- and 3-folds 24 and 48 h after EGCG treatment, respectively (Fig. 7B). Likewise, analysis of mitochondrial energy metabolism of EGCG-treated MSTO-211H cells, showed that both the mitochondrial ATP production induced by complexes I and II substrates (Fig. 7C) and the cell ATP content (Fig. 7D), increased 1 h after EGCG treatment and then progressively reduced up to 24 h. We show that in MSTO-211H, as in the case of REN cells, EGCG acts via an early impairment of the MRC complexes, being their activity, in particular that of complex I, II and ATP synthase, already decreased 3 h after the treatment and reaching a 50% inhibition 24 h after treatment (Fig. 7E).

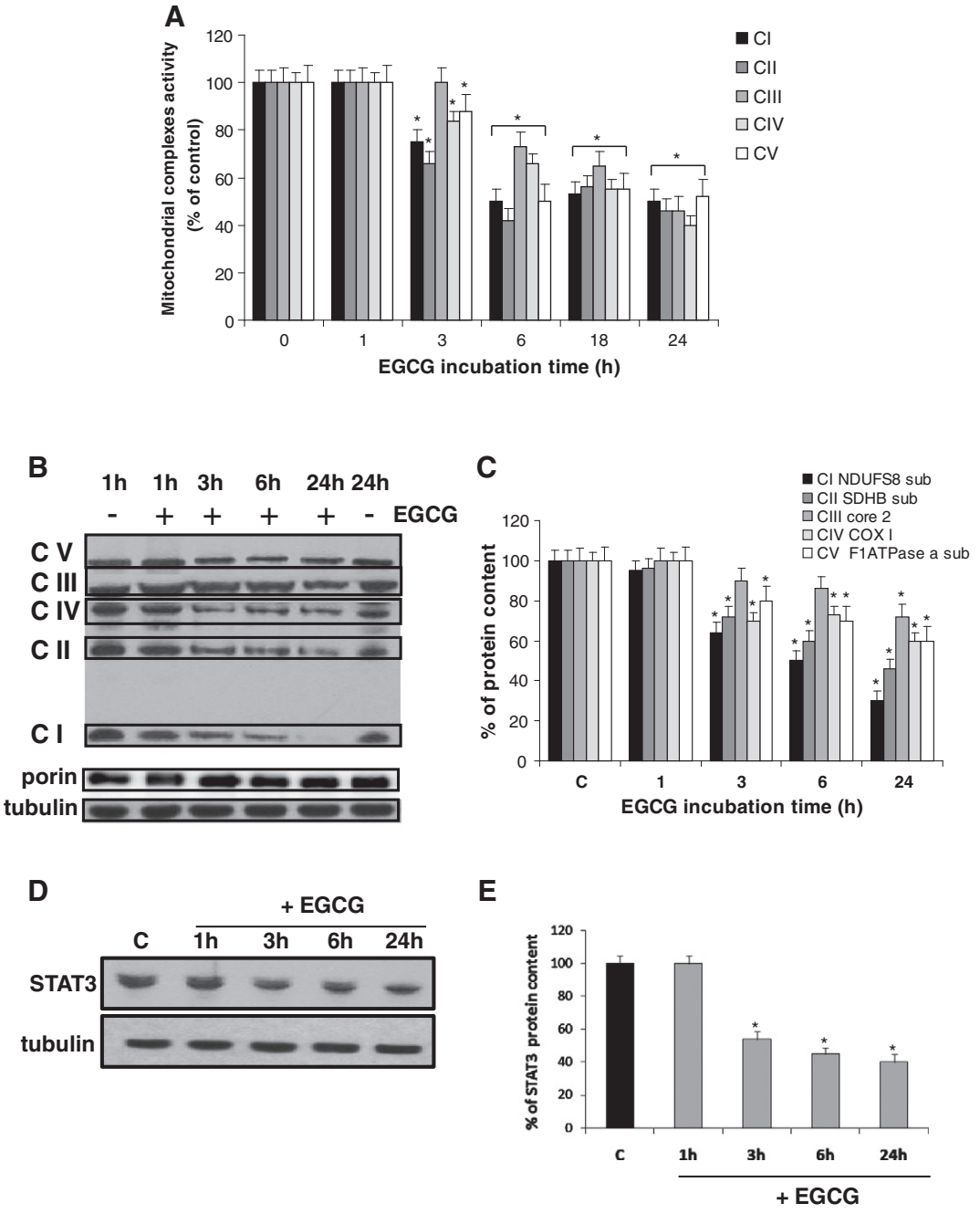

Fig. 5. Stabilized EGCG induces an early impairment of MRC complexes in MMe REN cells. Cells were treated with 100 μM EGCG in presence of SOD and CAT and collected at the indicated time periods. (A) The activities of respiratory complexes were measured spectrophotometrically in mitochondrial membrane-enriched fractions and expressed as a percentage of untreated control REN cells. (B) Representative immunoblotting and (C) densitomentric analysis of 20-kDa subunit of complex I (CI), 30-kDa subunit of complex II (CII), core 2 protein of complex III (CIII), COX I of complex IV (CIV) and α subunit of F_1 ATPase (CV) in untreated REN lysates collected after 1 and 24 h of incubation and EGCG-treated REN lysates obtained during the 24 hour period of treatment; protein levels of porin and tubulin as mitochondrial and cytosolic protein markers, respectively, were also analyzed. (D) Representative immunoblotting and (E) densitomentric analysis of STAT3 in untreated (C) and EGCG-treated REN extracts. The levels of the analyzed proteins normalized *vs* tubulin, are expressed as the percentage of untreated control cells. Graph is representative of four independent experiments. Each bar represents mean ± SD. Significant differences between untreated and treated cells are indicated with asterisks (* = $P < 0.05$).

4. Discussion

EGCG is a very multifunctional molecule known for its beneficial effects in a broad range of diseases including neurodegenerative and cardiovascular diseases [42–45], as well as cancer (for Refs. see [10,46]). In pathological conditions in which a deficit in OXPHOS is present, as in the case of Down syndrome, EGCG exerts a cytoprotective effect at low concentrations (10–20 μM), activating the mitochondrial energy metabolism [43]. Conversely, in several cancer types EGCG, used at higher concentrations, becomes cytotoxic and exerts an inhibitory action on cell proliferation [10,46,47]; however, studies on the effect of EGCG on mitochondrial energy metabolism in cancer cells are lacking. Here we report a molecular and functional study which shows for the first time that EGCG, *in vitro* stabilized with SOD/CAT, selectively induces apoptosis in

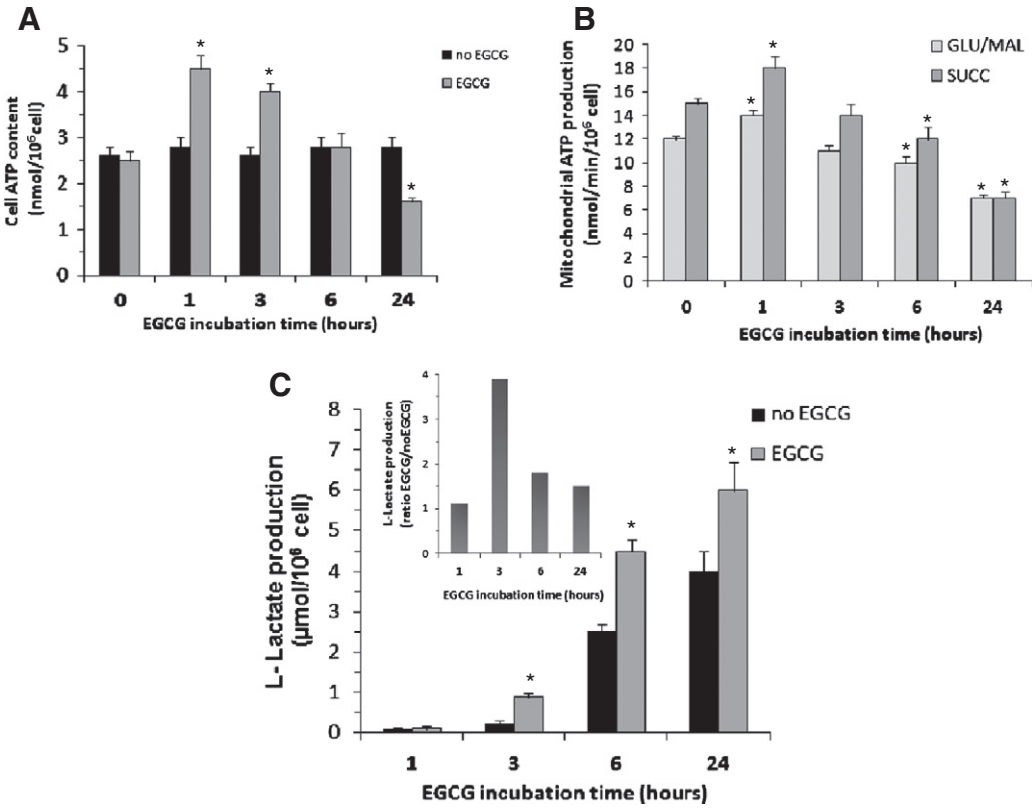

Fig. 6. Energy status in EGCG-treated MMe REN cells. Cells were treated with 100 μM EGCG in presence of SOD and CAT and collected at the indicated time periods. (A) ATP cellular levels were measured in cell extracts and expressed as nmol/10^6 cells. (B) The rate of mitochondrial ATP synthesis was measured spectrophotometrically as described in the Materials and methods, in the presence of either glutamate/malate (GLU/MAL) or succinate (SUCC) and expressed as nmol/min/10^6 cells. (C) Levels of L-lactate were measured in culture medium in both untreated and EGCG-treated REN and expressed as μmol/10^6 cells. The inset shows the ratio between the mean values of L-lactate level found in EGCG-treated and untreated cells. Graphs are representative of four independent experiments. Each bar represents mean ± SD. Significant differences between untreated and treated cells are indicated with asterisks (* = $P < 0.05$).

MMe cells, by decreasing MRC complex protein level and activity, impairing mitochondrial energy metabolism and leading to cellular ATP deficit and cell cycle arrest.

It has been recently shown that EGCG can undergo auto-oxidation causing a dose-dependent ROS production leading to cancer cell apoptosis [15–21]. In the present study, we show that EGCG added to cell culture medium induces a dose-dependent H_2O_2 formation and decreases the proliferation of both MMe REN and normal mesothelial MET5A cells to indicate that H_2O_2 generated from EGCG auto-oxidation might be responsible for its non-selective cytotoxicity. EGCG stabilized by SOD and CAT [20,21] which prevent H_2O_2 formation in culture medium, induces a selective inhibition of MMe REN cell growth with an IC_{50} value of 100 μM, without effects on MET5A cells. In addition, since SOD and CAT cannot cross the plasma membrane, the significant decrease in H_2O_2 intracellular levels observed in the presence of 100 μM EGCG plus SOD/CAT suggests that the stabilized EGCG acts as a powerful intracellular antioxidant and that the selective inhibition of MMe REN cell growth by EGCG takes place preventing pro-radical activity of the drug by its stabilization. Of course under this condition, i.e. in the absence of extracellular and cytoplasmic ROS, there is a slower induction of cell death than in the presence of non-stabilized EGCG. But in this latter case we cannot surely affirm that the induction of apoptosis, which occurs also in normal mesothelial MET5A cells, was due to EGCG or to its auto-oxidation products which produce themselves ROS. These results should be considered in future studies attempting to elucidate the mechanisms of action of EGCG *in vitro* systems also in the light of the observation that oxidation of EGCG does not seem to occur *in vivo* since none of EGCG oxidation products were found in the plasma samples of mice after treatment with EGCG [48].

It should be noted that, as reported in lung cancer cells treated with EGCG stabilized with SOD/CAT [17], a still evident amount of mitochondrial ROS is observed in stabilized EGCG-treated REN cells, probably due to the mitochondrial dysfunction. Consistently, EGCG treatment of MMe REN cells for 24 h results in a dose-dependent impairment of MRC complex activity. Here we provide indications aiming to account for the impairment of MRC complexes found in EGCG-treated MMe REN cells. In an early phase (3–6 h) of treatment, EGCG promotes a significant general decrease in both activity and protein levels of MRC complexes, suggesting a regulation at a transcriptional/translational level. Accordingly, we found a down-regulation by EGCG of STAT3, a transcription factor known to be involved in the regulation of MRC complex expression and activity [37]. STAT3 is a proto-oncogene constitutively activated in diverse human cancers including malignant mesotheliomas [49,50] and known to play a critical role in tumor cell survival, proliferation, migration, invasion, angiogenesis and inhibition of apoptosis [50,51]. Although some studies reported STAT3 as a negative regulator of MRC complexes [52,53], recently STAT3 was shown to support oncogenic transformation sustaining MRC activity and blocking mitochondrial permeability transition pore [37,54,55]. Consistently with our results, it has also been reported that EGCG induces a decrease in STAT3 protein level inhibiting its downstream signaling pathway and inducing apoptosis in human pancreatic cancer [37]. Here we show that a down-regulation of STAT3 occurs as a very early event following EGCG treatment suggesting STAT3 as a primary target of this molecule in MMe REN cells. Further studies are required to verify whether the EGCG-dependent STAT3 down-regulation correlates with the impairment of MRC complexes.

EGCG-treated REN cells show a significant shortage of mitochondrial ATP production, as well as a marked decline in cellular ATP levels. Given that a decrease in ATP levels likely affects a variety of vital cellular processes, including transcription, translation and signal transduction, it is noticeable to find REN cell cycle arrest. Furthermore, following the cell

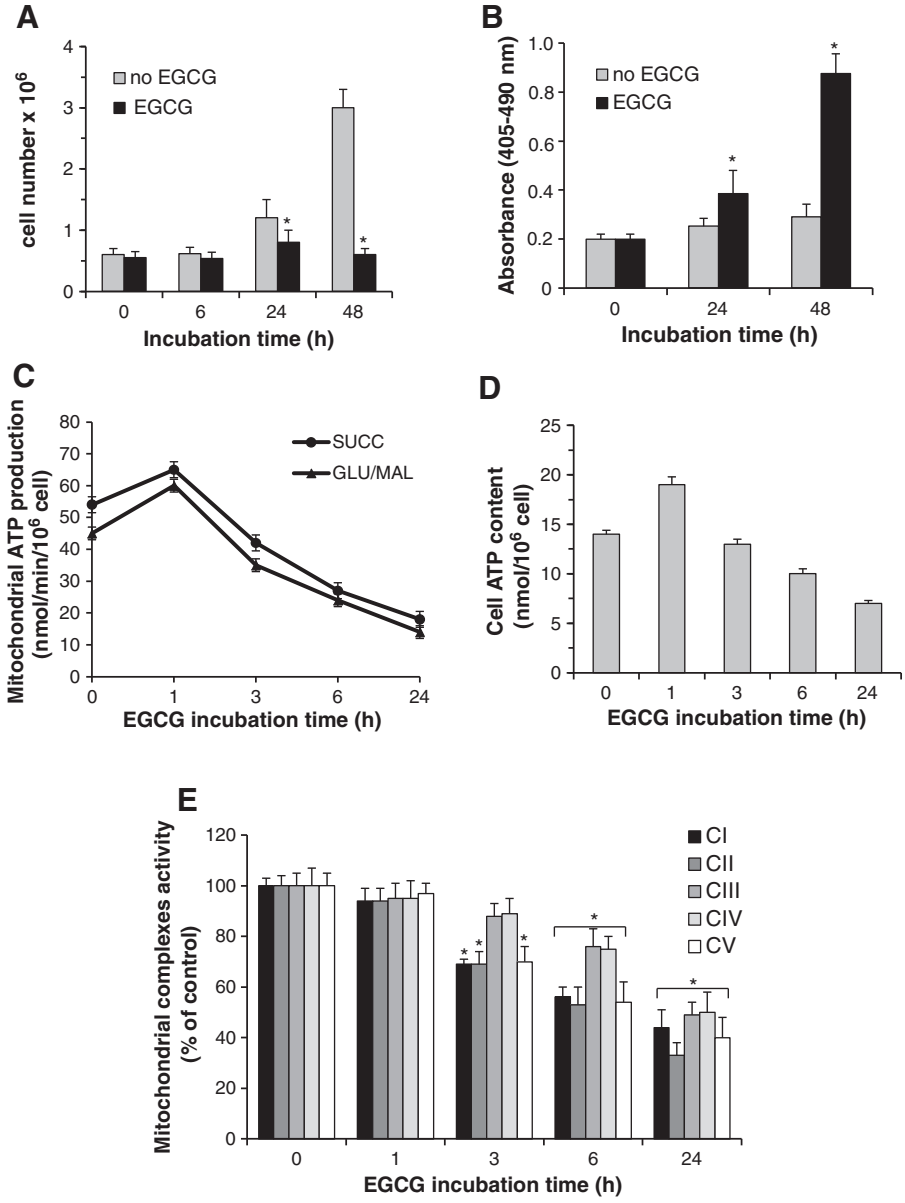

Fig. 7. Stabilized EGCG induces apoptosis in MSTO-211H MMe cells through an early impairment of mitochondrial energy metabolism and MRC complex activities. Cells were treated with 100 μM EGCG in presence of SOD and CAT and collected at the indicated time periods. Cell survival (A) and cell apoptosis (B) were measured as a function of time as described in the Materials and methods. Graphs are representative of three independent experiments. (C) The rate of mitochondrial ATP synthesis was measured spectrophotometrically as described in the Materials and methods, in the presence of either glutamate/malate (GLU/MAL) or succinate (SUCC) and expressed as nmol/min/10^6 cells. (D) ATP cellular levels were measured in cell extracts and expressed as nmol/10^6 cells. (E) The activities of respiratory complexes were measured spectrophotometrically in mitochondrial membrane-enriched fractions and expressed as a percentage of untreated control REN cells. In panels A, B and E significant differences between untreated and treated cells are indicated with asterisks ($* = P < 0.05$). In panels C and D all data obtained in 1–24-h time period are significantly different with respect to controls ($P < 0.05$). In panels C–E values obtained in untreated control cells are equal to that at 0-h and remained constant during the incubation time.

cycle arrest, EGCG-treated MMe REN cells show typical signs of apoptosis, such as histone-associated-DNA-fragmentation and nuclear chromatin margination. Drug-induced G2/M arrest followed by apoptosis occurs in a variety of tumor types of both epithelial and hematologic cell origin [56]. Interestingly, ultrastructural mitochondrial changes, such as cristae opening and mitochondrial swelling, as well as cyt *c* release by mitochondria, occur only 6 h after EGCG treatment when no signs of apoptosis are detectable, indicating that EGCG induces mitochondrial-mediated apoptosis in MMe REN cells.

The results reported in this paper shed a new light on some aspects of energy metabolism in EGCG-treated MMe cells. In the early phase of EGCG treatment (1–3 h), an increase in the ATP level occurs which derives from both anaerobic glycolysis and oxidative phosphorylation, as revealed from the increased L-lactate levels and the still efficient mitochondrial ATP production. This early cellular ATP surge might be a trigger to initiate the programmed cell death [39,40] or even a cytoprotective mechanism of resistance to chemotherapeutic agents [57]. In the late phase of EGCG treatment (18–24 h), when the oxidative phosphorylation is strongly impaired, cellular ATP level strongly decreases suggesting that the energy shift towards glycolysis is no more sufficient to maintain the energy demand, and MMe cells proceed towards cycle arrest and then apoptosis.

These data have been confirmed in cells derived from biphasic MMe, the MSTO-211H cell line which appeared to be even more sensitive than REN (epithelioid) MMe cell line to the growth-inhibitory effect of EGCG, probably due to the highly aggressive nature of MSTO-211H cells [41].

Interestingly, MSTO-211H cells showed a very high mitochondrial metabolism being both mitochondrial ATP production and ATP cellular level in basal condition (i.e. without EGCG treatment) about 4-fold higher than that observed in REN (compare Figs. 7 and 6) supporting the hypothesis of a correlation between enhanced OXPHOS and tumor proliferation in MMe as described in other tumor types [2–4].

Our results provide evidences supporting the use of EGCG as adjuvant in combination with other chemotherapic agents with proven efficacy on MMe cells such as gemcitabine, as proposed in [58], to be tested in experimental earlier phases of clinical trials. Moreover, it can be hypothesized that a local infusion of EGCG might help in preventing recurrent pleural effusion in patients with advanced disease.

In conclusion, the present report suggests that EGCG, as well as other agents that inhibit MRC complex activities and energy metabolism, may provide reliable therapeutic options for the management of MMe and may be useful in the treatment of malignant tumors.

Acknowledgements

This work was supported by the CNR Project "FaReBio di Qualità" and by Fondazione Buzzi Unicem. The authors thank Ms. Annarita Armenise for technical assistance.

References

[1] W.H. Koppenol, P.L. Bounds, C.V. Dang, Otto Warburg's contributions to current concepts of cancer metabolism, Nat. Rev. Cancer 11 (2011) 325–337.
[2] F. Weinberg, R. Hamanaka, W.W. Wheaton, S. Weinberg, J. Joseph, M. Lopez, B. Kalyanaraman, G.M. Mutlu, G.R. Budinger, N.S. Chandel, Mitochondrial metabolism and ROS generation are essential for Kras-mediated tumorigenicity, Proc. Natl. Acad. Sci. U. S. A. 107 (2010) 8788–8793.
[3] D. Whitaker-Menezes, U.E. Martinez-Outschoorn, N. Flomenberg, R.C. Birbe, A.K. Witkiewicz, A. Howell, S. Pavlides, A. Tsirigos, A. Ertel, R.G. Pestell, P. Broda, C. Minetti, M.P. Lisanti, F. Sotgia, Hyperactivation of oxidative mitochondrial metabolism in epithelial cancer cells in situ: visualizing the therapeutic effects of metformin in tumor tissue, Cell Cycle 10 (2011) 4047–4064.
[4] M. Barbi de Moura, G. Vincent, S.L. Fayewicz, N.W. Bateman, B.L. Hood, M. Sun, J. Suhan, S. Duensing, Y. Yin, C. Sander, J.M. Kirkwood, D. Becker, T.P. Conrads, B. Van Houten, S.J. Moschos, Mitochondrial respiration—an important therapeutic target in melanoma, PLoS One 7 (2012) e40690.
[5] Y. Li, D. Li, S. Yuan, Z. Wang, F. Tang, R. Nie, J. Weng, L. Ma, B. Tang, Embelin-induced MCF-7 breast cancer cell apoptosis and blockade of MCF-7 cells in the G2/M phase via the mitochondrial pathway, Oncol. Lett. 5 (2013) 1005–1009.
[6] B. Cunniff, K. Benson, J. Stumpff, K. Newick, P. Held, D. Taatjes, J. Joseph, B. Kalyanaraman, N.H. Heintz, Mitochondrial-targeted nitroxides disrupt mitochondrial architecture and inhibit expression of peroxiredoxin 3 and FOXM1 in malignant mesothelioma cells, J. Cell. Physiol. 228 (2013) 835–845.
[7] N.P. Campbell, H.L. Kindler, Update on malignant pleural mesothelioma, Semin. Respir. Crit. Care Med. 32 (2011) 102–110.
[8] S. Piyaviriyakul, K. Shimizu, T. Asakawa, T. Kan, P. Siripong, N. Oku, Anti-angiogenic activity and intracellular distribution of epigallocatechin-3-gallate analogs, Biol. Pharm. Bull. 34 (2011) 396–400.
[9] S. Hsu, J. Lewis, B. Singh, P. Schoenlein, T. Osaki, M. Athar, A.G. Porter, G. Schuster, Green tea polyphenol targets the mitochondria in tumor cells inducing caspase 3-dependent apoptosis, Anticancer. Res. 23 (2003) 1533–1539.
[10] J. Kanwar, M. Taskeen, I. Mohammad, C. Huo, T.H. Chan, Q.P. Dou, Recent advances on tea polyphenols, Front Biosci. 4 (2012) (2012) 111–131.
[11] S.K. Patra, F. Rizzi, A. Silva, D.O. Rugina, S. Bettuzzi, Molecular targets of (−)-epigallocatechin-3-gallate (EGCG): specificity and interaction with membrane lipid rafts, Physiol. Pharmacol. 59 (2008) 217–235.
[12] B.N. Singh, S. Shankar, R.K. Srivastava, Green tea catechin, epigallocatechin-3-gallate (EGCG): mechanisms, perspectives and clinical applications, Biochem. Pharmacol. 82 (2011) 1807–1821.
[13] S. Qanungo, M. Das, S. Haldar, A. Basu, Epigallocatechin-3-gallate induces mitochondrial membrane depolarization and caspase-dependent apoptosis in pancreatic cancer cells, Carcinogenesis 26 (2005) 958–967.
[14] I.S. Kil, K.H. Jung, W.S. Nam, J.W. Park, Attenuated mitochondrial NADP+-dependent isocitrate dehydrogenase activity enhances EGCG-induced apoptosis, Biochimie 93 (2011) 1808–1815.
[15] E. Ranzato, S. Martinotti, V. Magnelli, B. Murer, S. Biffo, L. Mutti, B. Burlando, Epigallocatechin-3-gallate induces mesothelioma cell death via H_2O_2-dependent T-type Ca^{2+} channel opening, J. Cell. Mol. Med. 16 (2012) 2667–2678.
[16] M. Satoh, Y. Takemura, H. Hamada, Y. Sekido, S. Kubota, EGCG induces human mesothelioma cell death by inducing reactive oxygen species and autophagy, Cancer Cell Int. 13 (2013) 19.
[17] G.X. Li, Y.K. Chen, Z. Hou, H. Xiao, H. Jin, G. Lu, M.J. Lee, B. Liu, F. Guan, Z. Yang, A. Yu, C.S. Yang, Pro-oxidative activities and dose-response relationship of (−)-epigallocatechin-3-gallate in the inhibition of lung cancer cell growth: a comparative study *in vivo* and *in vitro*, Carcinogenesis 31 (2010) 902–910.
[18] S. Azam, N. Hadi, N.U. Khan, S.M. Hadi, Prooxidant property of green tea polyphenols epicatechin and epigallocatechin-3-gallate: implications for anticancer properties, Toxicol. In Vitro 18 (2004) 555–561.
[19] L.H. Long, D. Kirkland, J. Whitwell, B. Halliwell, Different cytotoxic and clastogenic effects of epigallocatechin gallate in various cell-culture media due to variable rates of its oxidation in the culture medium, Mutat. Res. 634 (2007) 177–183.
[20] Z. Hou, S. Sang, H. You, M.J. Lee, J. Hong, K.V. Chin, C.S. Yang, Mechanism of action of (−)-epigallocatechin-3-gallate: auto-oxidation-dependent inactivation of epidermal growth factor receptor and direct effects on growth inhibition in human esophageal cancer KYSE 150 cells, Cancer Res. 65 (2005) 8049–8056.
[21] J. Hong, H. Lu, X. Meng, J.H. Ryu, Y. Hara, C.S. Yang, Stability, cellular uptake, biotransformation, and efflux of tea polyphenol (−)-epigallocatechin-3-gallate in HT-29 human colon adenocarcinoma cells, Cancer Res. 62 (2002) 7241–7246.
[22] A.M. Orengo, L. Spoletini, A. Procopio, R.E. Favoni, A. De Cupis, A. Ardizzoni, B. Castagneto, M. Ribotta, P.G. Betta, S. Ferrini, L. Mutti, Establishment of four new mesothelioma cell lines: characterization by ultrastructural and immunophenotypic analysis, Eur. Respir. J. 13 (1999) 527–534.
[23] W.R. Smythe, L.R. Kaiser, H.C. Hwang, K.M. Amin, J.M. Pilewski, S.J. Eck, J.M. Wilson, S.M. Albelda, Successful adenovirus mediated gene transfer in an in vivo model of human malignant mesothelioma, Ann. Thorac. Surg. 57 (1994) 1395–1401.
[24] C.P. LeBel, H. Ischiropoulos, S.C. Bondy, Evaluation of the probe 2′ 7′-dichlorofluorescin as an indicator of reactive oxygen species formation and oxidative stress, Chem. Res. Toxicol. 5 (1992) 227–231.
[25] P. Mukhopadhyay, M. Rajesh, G. Haskó, B.J. Hawkins, M. Madesh, P. Pacher, Simultaneous detection of apoptosis and mitochondrial superoxide production in live cells by flow cytometry and confocal microscopy, Nat. Protoc. 2 (2007) 2295–2301.
[26] R.A. Vacca, E. Marra, G. Loverro, E. Maiorano, A. Napoli, M. Lovecchio, L. Selvaggi, E. Perlino, Differential expression of beta 1c integrin messenger ribonucleic acid and protein levels in human endometrium and decidua during the menstrual cycle and pregnancy, J. Clin. Endocrinol. Metab. 88 (2003) 720–729.
[27] B. Chelli, A. Lena, R. Vanacore, E. Da Pozzo, B. Costa, L. Rossi, A. Salvetti, F. Scatena, S. Ceruti, M.P. Abbracchio, V. Gremigni, C. Martini, Peripheral benzodiazepine receptor ligands: mitochondrial transmembrane potential depolarization and apoptosis induction in rat C6 glioma cells, Biochem. Pharmacol. 68 (2004) 125–134.
[28] D. Valenti, G.A. Manente, L. Moro, E. Marra, R.A. Vacca, Deficit of complex I activity in human skin fibroblasts with chromosome 21 trisomy and overproduction of reactive oxygen species by mitochondria: involvement of the cAMP/PKA signalling pathway, Biochem. J. 435 (2011) 679–688.
[29] P. Bénit, S. Goncalves, E. Philippe Dassa, J.J. Brière, G. Martin, P. Rustin, Three spectrophotometric assays for the measurement of the five respiratory chain complexes in minuscule biological samples, Clin. Chim. Acta 374 (2006) 81–86.
[30] N.C. Yang, W.M. Ho, Y.H. Chen, M.L. Hu, A convenient one-step extraction of cellular ATP using boiling water for the luciferin–luciferase assay of ATP, Anal. Biochem. 306 (2002) 323–327.
[31] D. Valenti, A. Tullo, M.F. Caratozzolo, R.S. Merafina, P. Scartezzini, E. Marra, R.A. Vacca, Impairment of F1F0-ATPase, adenine nucleotide translocator and adenylate kinase causes mitochondrial energy deficit in human skin fibroblasts with chromosome 21 trisomy, Biochem. J. 431 (2010) 299–310.
[32] W. Walz, S. Mukerji, Lactate production and release in cultured astrocytes, Neurosci. Lett. 86 (1988) 296–300.
[33] S. Dröse, U. Brandt, Molecular mechanisms of superoxide production by the mitochondrial respiratory chain, Adv. Exp. Med. Biol. 748 (2012) 145–169.
[34] L. Galluzzi, O. Kepp, C. Trojel-Hansen, G. Kroemer, Mitochondrial control of cellular life, stress, and death, Circ. Res. 111 (2012) 1198–1207.
[35] J.D. Inacio, M.M. Canto-Cavalheiro, R.F. Menna-Barreto, E.E. Almeida-Amaral, Mitochondrial damage contribute to epigallocatechin-3-gallate induced death in *Leishmania amazonensis*, Exp. Parasitol. 132 (2012) 151–155.
[36] P. Monian, X. Jiang, Clearing the final hurdles to mitochondrial apoptosis: regulation post cytochrome C release, Exp. Oncol. 34 (2012) 185–191.
[37] S.N. Tang, J. Fu, S. Shankar, R.K. Srivastava, EGCG enhances the therapeutic potential of gemcitabine and CP690550 by inhibiting STAT3 signaling pathway in human pancreatic cancer, PLoS One 7 (2012) e31067.
[38] K. Szczepanek, Q. Chen, A.C. Larner, E.J. Lesnefsky, Cytoprotection by the modulation of mitochondrial electron transport chain: the emerging role of mitochondrial STAT3, Mitochondrion 12 (2012) 180–189.
[39] M.V. Zamaraeva, R.Z. Sabirov, E. Maeno, Y. Ando-Akatsuka, S.V. Bessonova, Y. Okada, Cells die with increased cytosolic ATP during apoptosis: a bioluminescence study with intracellular luciferase, Cell Death and Differ. 12 (2005) 1390–1397.
[40] A. Fassina, R. Cappellesso, V. Guzzardo, L. Dalla Via, S. Piccolo, L. Ventura, M. Fassan, Epithelial–mesenchymal transition in malignant mesotelioma, Mod. Pathol. 25 (2012) 86–99.
[41] A. Atlante, S. Giannattasio, A. Bobba, S. Gagliardi, V. Petragallo, P. Calissano, E. Marra, S. Passarella, An increase in the ATP levels occurs in cerebellar granule cells en route to apoptosis in which ATP derives from both oxidative phosphorylation and anaerobic glycolysis, Biochim. Biophys. Acta 1708 (2005) 50–62.
[42] C. Mak, Potential role of green tea catechins in various disease therapies: progress and promise, Clin. Exp. Pharmacol. Physiol. 39 (2012) 265–273.
[43] D. Valenti, D. De Rasmo, A. Signorile, L. Rossi, L. de Bari, I. Scala, B. Granese, S. Papa, R.A. Vacca, Epigallocatechin-3-gallate prevents oxidative phosphorylation deficit and promotes mitochondrial biogenesis in human cells from subject with Down's syndrome, Biochim. Biophys. Acta 1832 (2013) 542–552.
[44] N. Dragicevic, A. Smith, X. Lin, F. Yuan, N. Copes, V. Delic, J. Tan, C. Cao, R.D. Shytle, P.C. Bradshaw, Green tea epigallocatechin-3-gallate (EGCG) and other flavonoids

reduce Alzheimer's amyloid-induced mitochondrial dysfunction, J. Alzheimers Dis. 26 (2011) 507–521.
[45] M. Tanaka, J. Zhao, A. Suyama, T. Matsui, Epigallocatechin gallate promotes the vaso-relaxation power of the antiatherosclerotic dipeptide Trp-His in contracted rat aorta, J. Agric. Food Chem. 60 (2012) 9048–9054.
[46] C.S. Yang, H. Wang, Mechanistic issues concerning cancer prevention by tea catechins, Mol. Nutr. Food Res. 55 (2011) 819–831.
[47] J.D. Lambert, M.J. Lee, L. Diamond, J. Ju, J. Hong, M. Bose, H.L. Newmark, C.S. Yang, Dose-dependent levels of epigallocatechin-3-gallate in human colon cancer cells and mouse plasma and tissues, Drug Metab. Dispos. 34 (2006) 8–11.
[48] S. Sang, I. Yang, B. Buckley, C.T. Ho, C.S. Yang, Autoxidative quinone formation in vitro and metabolite formation in vivo from tea polyphenol (−)-epigallocatechin-3-gallate: studied by real-time mass spectrometry combined with tandem mass ion mapping, Free Radic. Biol. Med. 43 (2007) 362–371.
[49] P.A. Johnston, J.R. Grandis, STAT3 signaling: anticancer strategies and challenges, Mol. Interv. 11 (2011) 18–26.
[50] O. Achcar Rde, P.T. Cagle, J. Jagirdar, Expression of activated and latent signal transducer and activator of transcription 3 in 303 non-small cell lung carcinomas and 44 malignant mesotheliomas: possible role for chemotherapeutic intervention, Arch. Pathol. Lab. Med. 131 (2007) 1350–1360.
[51] A. Subramaniam, M.K. Shanmugam, E. Perumal, F. Li, A. Nachiyappan, X. Dai, S.N. Swamy, K.S. Ahn, A.P. Kumar, B.K. Tan, K.M. Hui, G. Sethi, Potential role of signal transducer and activator of transcription (STAT)3 signaling pathway in inflammation, survival, proliferation and invasion of hepatocellular carcinoma, Biochim. Biophys. Acta 1835 (2013) 46–60.
[52] M. Demaria, C. Giorgi, M. Lebiedzinska, G. Esposito, L. D'Angeli, A. Bartoli, D.J. Gough, J. Turkson, D.E. Levy, C.J. Watson, M.R. Wieckowski, P. Provero, P. Pinton, V. Poli, A STAT3-mediated metabolic switch is involved in tumour transformation and STAT3 addiction, Aging (Albany NY) 2 (2010) 823–842.
[53] M. Demaria, V. Poli, From the nucleous to the mitochondria and back. The odyssey of a multitask STAT3, Cell Cycle 10 (2011) 3221–3222.
[54] D.J. Gough, A. Corlett, K. Schlessinger, J. Wegrzyn, A.C. Larner, D.E. Levy, Mitochondrial STAT3 supports Ras-dependent oncogenic transformation, Science 324 (2009) 1713–1716.
[55] K. Boengler, D. Hilfiker-Kleiner, G. Heusch, R. Schulz, Inhibition of permeability transition pore opening by mitochondrial STAT3 and its role in myocardial ischemia/reperfusion, Basic Res. Cardiol. 105 (2010) 771–785.
[56] W. Xia, S. Spector, L. Hardy, S. Zhao, A. Saluk, L. Alemane, N.L. Spector, Tumor selective G2/M cell cycle arrest and apoptosis of epithelial and hematological malignancies by BBL22, a benzazepine, Proc. Natl. Acad. Sci. U. S. A. 97 (2000) 7494–7499.
[57] M. Katayama, T. Kawaguchi, M.S. Berger, R.O. Pieper, DNA damaging agent-induced autophagy produces a cytoprotective adenosine triphosphate surge in malignant glioma cells, Cell Death Differ. 14 (2007) 548–558.
[58] V. Volta, E. Ranzato, S. Martinotti, S. Gallo, M.V. Russo, L. Mutti, S. Biffo, B. Burlando, Preclinical demonstration of synergistic Active Nutrients/Drug (AND) combination as a potential treatment for malignant pleural mesothelioma, PLoS One 8 (2013) e58051.